COMMUNICATIONS IN COMPUTATIONAL PHYSICS
Vol. **3**, No. 4, pp. 878-898

Commun. Comput. Phys.
April 2008

PDE Constrained Optimization and Design of Frozen Mode Crystals

S. Chun and J. S. Hesthaven*

Division of Applied Mathematics, Brown University, Providence, RI 02912, USA.

Received 10 December 2006; Accepted (in revised version) 16 August 2007

Available online 11 December 2007

Abstract. We explore the use of PDE constrained nonlinear optimization techniques to optimize and design electromagnetic crystals which exhibit frozen mode behavior. This is characterized by Van Hove singularities in the dispersion relation, e.g., stationary reflection points and degenerate band edge points. Hence, the optimization process modifies the dispersion relation by adjusting the geometries and material parameters. The resulting algorithm is found to be capable of recovering all known crystal configurations as well as many new configurations, some of which display dramatically improved properties over previously used configuration. We investigate both gyrotropic photonic crystals and degenerate band edge crystals as well as the more complex case of the oblique incidence. In this latter case, we extend the investigation to the three-dimensional case to identify the first three-dimensional crystal exhibiting frozen mode behavior.

AMS subject classifications: 65M60, 78A48, 78M10, 93M25

Key words: PDE constrained optimization, method of matched asymptotics, frozen mode, photonic crystal.

1 Introduction

Controlling the flow of electromagnetic waves in materials has been at the frontier of significant research efforts during the last decade. Well known examples rely on the ability to prohibit wave propagation or generation of strongly localize electromagnetic energy, both utilized in photonic bandgap devises. Furthermore, recent studies of periodic structures of anisotropic materials have demonstrated the ability to produce unexpected electromagnetic phenomena such as a dramatic slow-down of the wave and a significant increase in field amplitude without adversely affecting the ability to transmit energy

*Corresponding author. *Email addresses:* schun@dam.brown.edu (S. Chun), Jan.Hesthaven@Brown.edu (J. S. Hesthaven)

into these crystals [3–5]. Under ideal circumstances, this has been shown to a allow a dramatic compression of the electromagnetic energy inside the crystal with a vanishing group velocity at the carrier frequency. This phenomenon has been called a frozen mode and these unique features of this are attractive for numerous practical applications. Recent studies [1] have confirmed the robustness of these phenomena, further increasing the practicality of manufacturing such devises.

Initially, the frozen mode was regarded as a distinctive phenomenon related to stationary inflection points of the dispersion relations $\omega(k)$ such as,

$$\frac{\partial\omega}{\partial k}=0;\quad \frac{\partial^2\omega}{\partial k^2}=0;\quad \frac{\partial^3\omega}{\partial k^3}\neq 0\quad \text{at } \omega=\omega_0.$$

These properties of the dispersion relation are special cases of what is known as Van Hove singularities [7] as points where the first derivative of the dispersion relation $\omega(k)$ vanishes, i.e.,

$$\frac{\partial\omega}{\partial k}=0\quad \text{at } \omega=\omega_0.$$

This nomenclature is related to the density of state (DOS), as it is known that the DOS is inversely proportional to $\partial\omega/\partial k$ [8].

All previous studies have focused on the analysis of crystal configurations found by a trial-and-error technique. Due to complexity of finding useful configurations, this clearly limits the number of parameters one can freely manage to vary. This naturally again impact that parameter space one can practically search and leaves open questions of whether it is generally possible to achieve the properties in the dispersion relation, e.g., given some specific materials, can modify the geometric properties of the crystal as needed?

To address this problem in a more systematic way, we consider the implementation of a PDE constrained optimization approach where we use the dispersion relation, given by the transfer matrix method or by solving the Maxwell eigenproblem, in combination with the algorithm of Method of Moving Asymptote (MMA) [9–13]. This allows us to recreate and to optimize known configurations as well as to design entirely new crystal arrangements.

We consider the optimization and design of three different types of crystals all of which exhibit the frozen mode phenomena. The first one is a gyrotropic photonic crystal consisting of two misaligned anisotropic layers and one magnetic layer. Its dispersion relation has a stationary inflection point in the 2nd band. The second class of crystals consists of two misaligned anisotropic layers and vacuum between them. Its dispersion relation has a degenerate band edge in the first band. The final structure consists of only one anisotropic layer with $\varepsilon_{xz}\neq 0$ and vacuum between them. However, the frozen mode phenomenon only emerges when the incident wave propagates into this layer at an oblique angle. This latter case is quite different from the previous two cases. The dispersion relation was originally computed by a one-dimensional transfer matrix method

with certain assumptions on the wave vector. To verify the existence of a stationary inflection point in a general three dimensional setting, something which was previously unascertained, we solve the general three-dimensional Maxwell eigenproblem to get the dispersion relation with the quasi-three-dimensional initial parameter sets and apply the optimization techniques to seek a stationary inflection point in the three-dimensional dispersion relation. These new parameters are then used in a time-domain simulation to validate the genuine three-dimensional frozen mode phenomenon.

The remaining part of the paper is organized as follows. In Section 2, we briefly recall the physical model, Maxwell's equations and how one recovers the dispersion relation from these equations. This sets the stage for the implementation of the optimization method based on Method of Moving Asymptote. In Sections 3 and 4, we explore the methods and show results of optimizing the magnetic frozen mode and degenerate band edge for previously known designs as well as new configurations. Section 5 is devoted to the design of crystals for the oblique case. We conclude with a few remarks and directions for future works in Section 6.

2 Physical model

We consider Maxwell's equations

$$\nabla\times\tilde{\mathbf{E}}=-\frac{d\tilde{\mathbf{B}}}{dt},\quad \nabla\times\tilde{\mathbf{H}}=\frac{d\tilde{\mathbf{D}}}{dt},$$

where $\tilde{\mathbf{E}}$ and $\tilde{\mathbf{H}}$ are the electric field and magnetic field, respectively, and $\tilde{\mathbf{D}}$ and $\tilde{\mathbf{B}}$ the displacement field and the induction field. These fields are related by linear constitutive relations as

$$\tilde{\mathbf{D}}(z)=\hat{\varepsilon}(z)\tilde{\mathbf{E}}(z),\quad \tilde{\mathbf{B}}(z)=\hat{\mu}(z)\tilde{\mathbf{H}}(z),$$

where we have assumed that $(\hat{\varepsilon},\hat{\mu})$ are homogeneous in the (x,y)-plane. If we consider harmonic solutions at frequency ω, we recover Maxwell's equations in the frequency domain

$$\nabla\times\tilde{\mathbf{E}}=i\omega\hat{\mu}(z)\tilde{\mathbf{H}},\quad \nabla\times\tilde{\mathbf{H}}=-i\omega\hat{\varepsilon}(z)\tilde{\mathbf{E}}. \tag{2.1}$$

To simplify the above equations, we introduce the normalized quantities using

$$z=\frac{\tilde{z}}{\tilde{L}},\quad t=\frac{\tilde{t}}{\tilde{L}/\tilde{c_0}},$$

where $\tilde{L}$ is a reference length and $\tilde{c_0}=(\tilde{\varepsilon}_0\tilde{\mu}_0)^{-\frac{1}{2}}$ is the dimensional speed of light in vacuum. Also, $\tilde{\mathbf{E}}$ and $\tilde{\mathbf{H}}$ are normalized as

$$\mathbf{E}=\sqrt{\frac{\tilde{\varepsilon_0}}{\tilde{\mu_0}}}\frac{\tilde{\mathbf{E}}}{\tilde{H}_0},\quad \mathbf{H}=\frac{\tilde{\mathbf{H}}}{\tilde{H}_0},$$

where $\tilde{H}_0$ is a dimensional reference magnetic field strength. This yields the non-dimensionalized equations

$$\nabla\times\mathbf{E}=i\omega\hat{\mu}(z)\mathbf{H},\quad \nabla\times\mathbf{H}=-i\omega\hat{\varepsilon}(z)\mathbf{E},$$

where $(\hat{\varepsilon},\hat{\mu})$ now represent the relative permittivity and permeability, respectively.

Let us assume that the solution is periodic of the form

$$\begin{bmatrix}\vec{E}(\vec{x})\\ \vec{H}(\vec{x})\end{bmatrix}=\begin{bmatrix}\vec{E}_k\\ \vec{H}_k\end{bmatrix}\exp(i\vec{k}\cdot\vec{x}),\quad \vec{k}=\text{wave vector}.$$

Then, we recover the modal equation

$$(\nabla+i\vec{k})\times\mathbf{E}_k=i\omega\hat{\mu}(z)\mathbf{H}_k,\quad (\nabla+i\vec{k})\times\mathbf{H}_k=-i\omega\hat{\varepsilon}(z)\mathbf{E}_k,$$

which simplifies as

$$(\nabla+i\vec{k})\times\frac{1}{\hat{\mu}(z)}(\nabla+i\vec{k})\times\mathbf{E}_k=\omega^2\hat{\varepsilon}(z)\mathbf{E}_k. \tag{2.2}$$

For a given value of the wave vector $\vec{k}$, the above problem is recognized as an eigenvalue problem for $(\omega^2,\mathbf{E}_k)$, from which we recover the dispersion relation $(\vec{k},\omega(\vec{k}))$.

When optimizing the crystals, we must ensure that the solutions satisfy the above eigenvalue problem which emerges as the constraints in the optimization process.

The goal of the optimization is to identify Van Hove singularities [7] in the dispersion relation, leading to a very strong divergence of the density of states (DOS) near the corresponding frequency. There are several types of such singularities, but we are mainly interested in singularities where the first and second derivative are both zero, i.e.,

$$\frac{\partial\omega}{\partial k}=0,\quad \frac{\partial^2\omega}{\partial k^2}=0,\quad \text{at } \omega=\omega_0.$$

We state this equivalently as the following minimization problem:

$$\begin{aligned}\text{minimize}\quad & \lambda\left|\frac{d\omega}{dk}(\vec{x})\right|+\left|\frac{d^2\omega}{dk^2}(\vec{x})\right|,\quad \text{at } \vec{k}=\vec{k}_0,\\ & x_j^{min}\le x_j\le x_j^{max},\quad 1\le j\le n,\quad n=\text{number of variables},\end{aligned} \tag{2.3}$$

where $\vec{x}$ is a n-variable vector and $|\cdot|$ means the absolute value of the scalar $d\omega/dk$ and $d^2\omega/dk^2$. Here, λ is a weight which is dependent on the type of singularities. The objective function $d\omega/dk\,(\vec{x})$ and $d^2\omega/dk^2\,(\vec{x})$ can be obtained directly from the dispersion relation with optimization variable $\vec{x}$ by solving the eigenvalue problem in Eq. (2.2). Once the dispersion relation is obtained, the derivatives of the objective functions can be computed. Jacobians and Hessians needed in the evaluation of the objective function are

computed using fourth order finite difference approximation as

$$\frac{d}{dx}\left\{\frac{d\omega}{dk}(x_j)\right\}=\frac{1}{12\Delta x}\left\{-\frac{d\omega_{j+2}}{dk}+8\frac{d\omega_{j+1}}{dk}-8\frac{d\omega_{j-1}}{dk}+\frac{d\omega_{j-2}}{dk}\right\},$$
$$\frac{d^2}{d^2}\left\{\frac{d\omega}{dk}(x_j)\right\}=\frac{1}{12(\Delta x_j)^2}\left\{-\frac{d\omega_{j+2}}{dk}+16\frac{d\omega_{j+1}}{dk}-30\frac{d\omega_j}{dk}+16\frac{d\omega_{j-1}}{dk}-\frac{d\omega_{j-2}}{dk}\right\},$$

where

$$\frac{d\omega_j}{dk}=\frac{d\omega}{dk}(x_j),\quad 1\le j\le n.$$

The fourth-order approximation is preferred in the computation of the derivatives to increase the accuracy and is also found to lead to a faster convergence. The extension to deal with more independent parameters is done through tensor products of the above scheme.

It is furthermore required to obtain an initial guess $\vec{k}_0$ or better yet a group of possible regions of wave vectors where we should seek to optimize the dispersion relation. This process of identifying suitable initial wave vectors is critical and significantly convergence of the optimization process. We use the following approach

1. Divide the dispersion relation into several sections where each section contains only one wave vector with
$$|\frac{d\omega}{dk}(\vec{x})|<\varepsilon\ll 1.$$
2. For each of these sections, identify, if possible, one wave vector, $\vec{k}_0$, such that
$$\min_j\left|\sum_{\ell=-2}^{2}\frac{d\omega_j}{dk}(\vec{k}_\ell)\right|\le\varepsilon. \tag{2.4}$$
The function inside the bars is a way of indicating the amount of the first and the second derivative at the same time
3. Optimize the objective function at this wave number, $\vec{k}_0$.

Since the objective function is generally not convex, we use the algorithm of Method of Moving Asymptote (MMA). The application of MMA to find singularity points of dispersion relation can be stated briefly as follows. First, Eq. (2.2) can be changed into the following equivalent problem:

$$\begin{aligned}
&\text{minimize} && f_0(x)=z+\sum_{i=1}^{4}c_iy_i \qquad (2.5)\\
&\text{subject to} && f_1(x)=\lambda\frac{d\omega}{dk}(\vec{x})-y_1\le 0,\quad f_2(x)=\frac{d^2\omega}{dk^2}(\vec{x})-y_2\le 0,\\
& && f_3(x)=-\lambda\frac{d\omega}{dk}(\vec{x})-y_3\le 0,\quad f_4(x)=-\frac{d^2\omega}{dk^2}(\vec{x})-y_4\le 0,\\
& && z\ge 0,\quad y_i\ge 0,\quad 1\le i\le 4,\\
& && x_j^{min}\le x_j\le x_j^{max},\quad 1\le j\le n,
\end{aligned}$$

where $y_1,\cdots,y_n$ and z are artificial optimization variables. Note that z is zero and y_i attains the maximum of each constraint function at the optimized solution $\vec{x}$. Now, we have the non-linear optimization problem with several constraints. For $f_i(\vec{x})$, we define $g_i(x)$ in the following way,

$$\begin{aligned} &g_i(x)=r_i+\sum_{j=1}^{n}\left(\frac{p_{ij}}{U_j-x_j}+\frac{q_{ij}}{x_j-L_j}\right),\\ &p_{ij}=\max\{0,(U_j-x_j)^2\frac{\partial f_i}{\partial x_j}\},\quad q_{ij}=\max\{0,-(x_j-L_j)^2\frac{\partial f_i}{\partial x_j}\},\\ &r_i=f_i(x)-\sum_{j=1}^{n}\left(\frac{p_{ij}}{U_j-x_j}+\frac{q_{ij}}{x_j-L_j}\right),\quad 1\le i\le 4,\quad 1\le j\le n. \end{aligned} \tag{2.6}$$

The parameters L_j and U_j (known as *moving asymptotes*) are chosen as $L_j<x_j<U_j$ and play a critical role in the convergence of the optimization scheme. In fact, L_j and U_j are adjusted for each iteration according to the convergence behavior of the scheme. Note that the second derivatives of g_i are given as

$$\frac{\partial^2 g_i}{\partial x_j x_\ell}=\delta_{j\ell}\left(\frac{2p_{ij}}{(U_j-x_j)^3}+\frac{2q_{ij}}{(x_j-L_j)^3}\right),\quad 1\le j,\quad \ell\le n.$$

Since $p_{ij}\ge 0$, $q_{ij}\ge 0$, g_i is a convex function. In fact, as long as L_j and U_j are finite, g_i is strictly convex in all variables except for $\partial g_i/\partial x_j\,(x)=0$, $1\le j\le n$. With g_i defined as in Eq. (2.6), we have the following subproblem.

$$\begin{aligned} &\text{minimize} && \sum_{j=1}^{n}\left(\frac{p_{ij}}{U_j-x_j}+\frac{q_{ij}}{x_j-L_j}\right)+r_0\\ &\text{subject to} && \left(\frac{p_{ij}}{U_j-x_j}+\frac{q_{ij}}{x_j-L_j}\right)+r_i\le f_i,\quad 1\le i\le 4,\\ & && x_j^{min}\le x_j\le x_j^{max},\quad 1\le j\le n. \end{aligned} \tag{2.7}$$

The Lagrangian function corresponding to this problem is given by

$$W(x,y)=\vec{r}_0-\vec{y}^T\vec{r}+\sum_{j=1}^{n}\left(\frac{p_{0j}+\vec{y}^T\vec{p}_j}{U_j-x_j(\vec{y})}+\frac{q_{0j}+\vec{y}^T\vec{q}_j}{x_j(\vec{y})-L_j}\right),$$

where $W(x,y)$ is differentiable, smooth, and concave. Finally, the Lagrangian dual problem is given by

$$\begin{aligned} &\text{maximize} && W(x,y)=\vec{r}_0-\vec{y}^T\vec{r}+\sum_{j=1}^{n}\left(\frac{p_{0j}+\vec{y}^T\vec{p}_j}{U_j-x_j(\vec{y})}+\frac{q_{0j}+\vec{y}^T\vec{q}_j}{x_j(\vec{y})-L_j}\right)\\ &\text{subject to} && y\ge 0. \end{aligned} \tag{2.8}$$

This yields a nice convex optimization problem and it can be solved by a primal-dual Newton method. The details for this primal-dual method are given in [13].

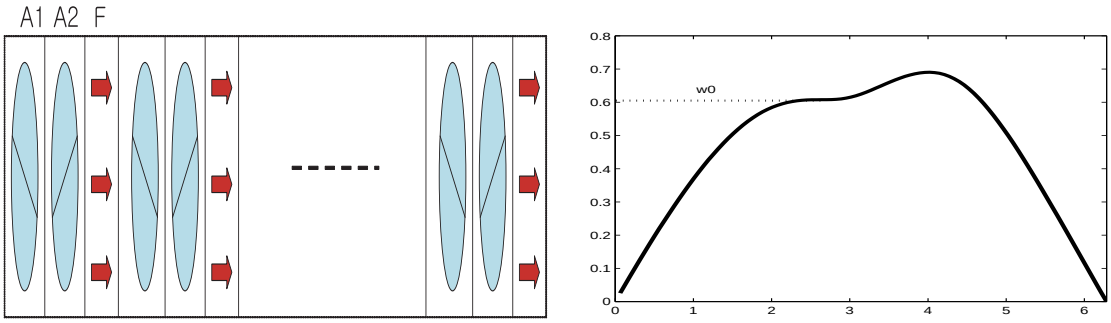

Figure 1: A periodic structure of gyrotropic photonic crystals consisting of two different anisotropic materials (A1,A2) with one magnetic layer (F) (left) and its dispersion relation (right).

3 Optimization and design of magnetic crystals

The frozen mode in the gyrotropic crystal occurs when a monochromatic wave with frequency ω_0 propagates into a periodic array consisting of two misaligned anisotropic layers and one magnetic layer as sketched in Fig. 1. In the dispersion relation there is a stationary inflection point with the following properties

$$\frac{\partial\omega}{\partial k}=0, \quad \frac{\partial^2\omega}{\partial k^2}=0, \quad \frac{\partial^3\omega}{\partial k^3}\neq 0, \qquad \text{at} \quad \omega=\omega_0. \tag{3.1}$$

As shown in [4], one set of parameters resulting in an inflection point at ω_0 is

- For the A layer:

$$\hat{\varepsilon}=\begin{bmatrix} 13.61+12.40\cos(2\phi) & 12.40\sin(2\phi) \\ 12.40\sin(2\phi) & 13.61-12.40\cos(2\phi) \end{bmatrix}, \quad \hat{\mu}=\hat{\mathbf{I}},$$

- For the F layer:

$$\hat{\varepsilon}=\begin{bmatrix} 5.0 & 0.0 \\ 0.0 & 5.0 \end{bmatrix}, \quad \hat{\mu}=\begin{bmatrix} 60.0 & i37.0 \\ -i37.0 & 60.0 \end{bmatrix},$$
$$\phi_1=0, \quad \phi_2=-\pi/4, \quad L_F=0.0047454, \quad L_A=0.5(1.0-\mathrm{L_F}),$$
$$k_0=2.6329, \quad \omega_0=0.607676756(c/L),$$

where ϕ_1 and ϕ_2 are the misalignment angle of the first and second anisotropic layer, respectively. Also, L_F is the thickness of the **F** layer and L_{A1}, L_{A2} are thickness of the first and second anisotropic layer, respectively.

The first task is to recover this set of parameters by the aforementioned optimization technique and, subsequently, seek other sets of parameters if possible. Since the periodicity is along z direction only, the dispersion relation of the magnetic frozen mode can be obtained by the transfer matrix method rather than solving the full Maxwell eigenvalue problem.

The transfer matrix method allows one to compute the dispersion relation from Bloch solutions of Maxwell's equations in planar structures. The transfer matrix ($T_L(\omega)$) can be obtained with bases of tangential components of electrical and magnetic fields. The Bloch solutions of the Maxwell's equations in a periodic media takes the form

$$q_k(z+L)=e^{ikL}q_k(z), \quad q_k=[E_x\ E_y\ H_x\ H_y]_k^T.$$

Using the property of transfer matrix $T_L(\omega)q_k(z)=q_k(z+L)$, we get the following characteristic equation

$$(T_L(\omega)-e^{ikL})q_k(L)=0 \implies \det(T_L(\omega)-e^{ikL})=0,$$

which yields the dispersion relation between ω and the wave vector k. The transfer matrix of an anisotropic layer with misalignment angle ϕ (T_A) and a magnetic layer (T_F) are given as

$$T_A(\phi,L_A)=W(\phi,L_A)W^{-1}(\phi,0), \quad T_F(L_F)=W(L_F)W^{-1}(0),$$

$$W(\phi,L_A)=\begin{bmatrix} (\cos\phi)e^{in_1a} & (\cos\phi)e^{-in_1a} & -(\sin\phi)e^{in_2a} & -(\sin\phi)e^{-in_2a} \\ (\sin\phi)e^{in_1a} & (\sin\phi)e^{-in_1a} & (\cos\phi)e^{in_2a} & (\cos\phi)e^{-in_2a} \\ -\eta_1(\sin\phi)e^{in_1a} & \eta_1(\sin\phi)e^{-in_1a} & -\eta_2(\cos\phi)e^{in_2a} & \eta_2(\cos\phi)e^{-in_2a} \\ \eta_1(\cos\phi)e^{in_1a} & -\eta_1(\cos\phi)e^{-in_1a} & -\eta_2(\sin\phi)e^{in_2a} & \eta_2(\sin\phi)e^{-in_2a} \end{bmatrix},$$

$$W(L_F)=\begin{bmatrix} e^{in_1f} & e^{-in_1f} & -ie^{in_2f} & -ie^{-in_2f} \\ -ie^{in_1f} & -ie^{-in_1f} & e^{in_2f} & e^{-in_2f} \\ i\eta_1e^{in_1f} & -i\eta e^{-in_1f} & -\eta_2e^{in_2f} & \eta_2e^{-in_2f} \\ \eta_1e^{in_1f} & -\eta e^{-in_1f} & -i\eta_2e^{in_2f} & i\eta_2e^{-in_2f} \end{bmatrix},$$

where $a=\omega L_A/c$ and $f=\omega L_F/c$. The transfer matrix of a three-cell layer is

$$T_L(\phi1,\phi2,L_{A1},L_{A2},L_F)=T_F(L_F)T_A(\phi_2,L_{A2})T_A(\phi_1,L_{A1})$$

and the dispersion relation of this layer is obtained by solving

$$\det(T_L-\xi\mathbf{I})=0, \quad \xi=e^{ikL}, \quad L=L_{A1}+L_{A2}+L_F.$$

This results in a fourth-order polynomial and we can compute its roots by simple root-finding methods.

As for choosing the wave vector k_0 corresponding to ω_0, we first find the wave vector k_b corresponding to a band edge (the highest peak such that $d\omega/dk|_{\omega=\omega_b}=0$) and seek a wave vector k less than the wave vector at the band edge where Eq. (2.4) attains a minimum. This may still miss candidates of a wave vector k_0 for optimized solution ω_0. To address this issue, we change the initial values if the converged solution does not satisfy

$$\frac{d\omega}{dk}<\varepsilon_1, \quad \frac{d^2\omega}{dk^2}<\varepsilon_2 \qquad \text{for sufficiently small } \varepsilon_1,\ \varepsilon_2.$$

In general, we shall allow the thickness of the magnetic layer (L_F), the thickness of the first anisotropic layer (L_{A1}) and material constants of the anisotropic layer (ε_A,δ_A) to vary during the optimization, although this could be extended to any number of parameters. In Fig. 2, we show the sequence of convergence of the dispersion relation for a known stationary inflection point using optimization with just one variable L_F.

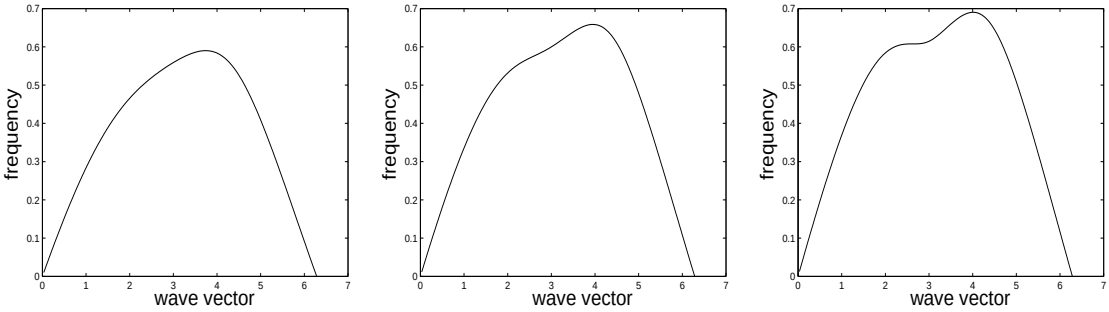

Figure 2: Snapshots from the optimization process with one variable L_F. Let $\rho_0 = L_A/L_F$. ρ_0=0.05 (left), 0.0.018924 (center), 0.0.0095342 (right) after 6 iterations, $\frac{d\omega}{dx}$= 3.97e-13, $\frac{d^2\omega}{dx^2}$= 0.007907 with $\lambda = 10000$ in Eq. (2.3).

Table 1: Optimized solutions with different number of variables (n) or different initial values for magnetic frozen mode. ϕ_2=misalignment angle of second anisotropic layer (we let $\phi_1 = 0$). L_F= thickness of magnetic layer, L_{A1}=thickness of the first anisotropic layer. TR (Transmittance) = I_T/I_I, $I \equiv \mu_0^{-1} < E \times B >$, $<>$ = time average over a period.

		Set 1	Set 2	Set 3	Set 4
Input	n	1	2	2	4
	variables	$L_F(L_{A1}=L_{A2})$	L_F,L_{A1}	L_F,L_{A1}	L_F,L_{A1},ε_A, δ_A
	ϕ_2	$-\pi/4$	$-\pi/4$	$-\pi/3$	$-\pi/4$
Solution	L_F	0.00474	0.00480	0.00490	0.00470
	L_{A1}	0.49763	0.44555	0.22056	0.45001
	ε_A	5.1	5.1	5.1	5.0
	δ_A	1.1	1.1	1.1	1.18189
	ω_0	0.60769	0.60950	0.67177	0.62171
	k_0	2.63894	2.63894	2.70177	2.63894
	$\frac{d\omega}{dk}\|_{\omega=\omega_0}$	3.9666e-13	2.41590e-16	6.5758e-16	1.80310e-12
	$\frac{d^2\omega}{dk^2}\|_{\omega=\omega_0}$	0.007907	0.00898	0.00917	0.00191
	TR	0.3388	0.4081	0.7786	0.3109

We note that the optimized solution for L_F is accurate up to 5.0e-06 with the analytically derived L_F [4] and the difference is negligible in the sense of sensitivity. Other optimized solutions with different number of variables (n) are shown in Table 1. In Table 1, ε_A and δ_A are used in the permittivity of anisotropic layer as follows:

$$\hat{\varepsilon} = \begin{bmatrix} \varepsilon_A + \delta_A \cos(2\phi) & \delta_A \sin(2\phi) \\ \delta_A \sin(2\phi) & \varepsilon_A - \delta_A \cos(2\phi) \end{bmatrix}.$$

We observe that the thickness of the **F** layer is approximately the same for all sets, but the thickness of the **A** layer varies depending on the misalignment angle or the material constants. The absolute values of the first and second derivative at each ω_0 are sufficiently close to zero to ensure that all sets show the characteristics of the frozen mode.

However, the closer to zero the first derivative is, the slower the group velocity of the wave is. Also, the intensity of the field amplitude inside the layer and the amount of energy density inside the layer are both closely related to the transmittance. A higher transmittance allows a larger fraction of the wave energy to enter into the crystal, resulting in a faster growth of the field amplitude and an increased energy density inside the crystal as illustrated in Fig. 3.

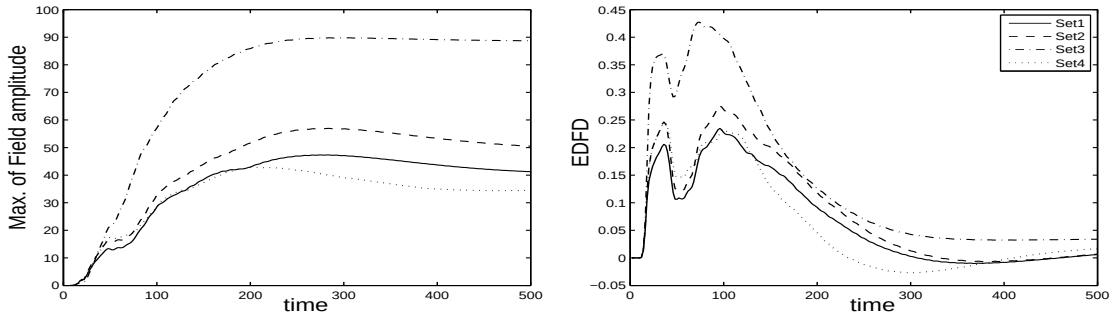

Figure 3: Maximum of the field amplitude (left) and the Energy Density flux difference (e_f of the first cell - e_f of the last cell, e_f=energy density flux) (right) for set 1 (solid line), set 2 (dashed line), set 3 (dot-dashed line) and set 4 (dotted line) of Table 1. Number of cells is 16 and an E$\|$x polarization of the incident field.

4 Optimization and design of degenerate band edge crystals

In the case of degenerate band edge crystals, the frozen mode behavior is associated with, in addition to the two first vanishing derivatives in the dispersion relation, a vanishing third derivative of the dispersion relation, i.e.,

$$\frac{\partial\omega}{\partial k}=0, \quad \frac{\partial^2\omega}{\partial k^2}=0, \quad \frac{\partial^3\omega}{\partial k^3}=0, \quad \text{at } \omega=\omega_0.$$

It is illustrated in Fig. 4.

Following [17], the following set of parameters generates a degenerate band edge point at $k_0=\pi$. For the A layer:

$$\hat{\varepsilon}=\begin{bmatrix} 13.61+12.40\cos(2\phi) & 12.40\sin(2\phi) \\ 12.40\sin(2\phi) & 13.61-12.40\cos(2\phi) \end{bmatrix}, \quad \hat{\mu}=\mathbf{I},$$
$$\phi_1=0, \quad \phi_2=\pi/4, \quad \mathrm{L_V}=0.45891, \quad \mathrm{L_A}=0.5(1.0-\mathrm{L_V}), \quad L=2L_A+L_V,$$
$$k_0=\pi, \quad \omega_0=1.0094052895(c/L),$$

where L_A and L_V are the thicknesses of the anisotropic layer and the vacuum layer, respectively. One of main advantages of this configuration is the absence of magnetic component which is both complicated and difficult to manufacture with a sufficiently low loss. As shown in Fig. 4, the dispersion relation is indeed flat at the degenerate band edge point.

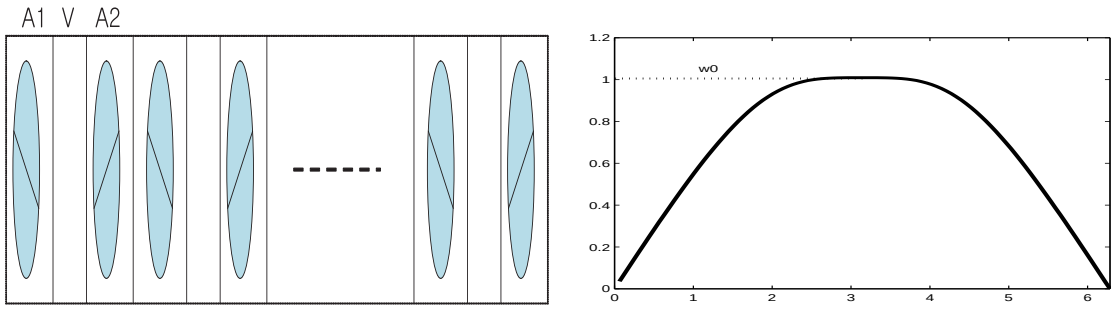

Figure 4: A periodic crystal structure allowing a degenerate band edge. The crystal consists of two misaligned anisotropic layers (A1,A2) with vacuum (V) between them (left). On the right we show the dispersion relation based on the parameters discussed in the text.

Similar to the previous magnetic case, the one-dimensional nature of the problem enables the use of the transfer matrix method, which is expressed as follows

$$T_L(\phi 1,\phi 2,L_{A1},L_{A2},L_V)=T_A(\phi_2,L_{A2})T_V(L_V)T_A(\phi_1,L_{A1}),$$

where

$$T_V(L_V)=W(L_V)W^{-1}(0),$$
$$W(L_V)=\begin{bmatrix} e^{iv} & e^{-iv} & -e^{ivf} & -e^{-iv} \\ e^{iv} & e^{-iv} & e^{iv} & e^{-iv} \\ -e^{iv} & e^{-iv} & -e^{iv} & e^{-iv} \\ e^{iv} & -e^{-iv} & -e^{iv} & e^{-iv} \end{bmatrix},$$

and $v=\omega L_V/c$. The structure of the periodic array shown in Fig. 4 always displays a degenerate band edge at $k_0=\pi$ independent of input parameters, so we do not need to find another candidates sets of k_0. As for the optimization of parameters, similar to magnetic frozen mode, we consider the thickness of the vacuum layer (L_V), the thickness of the first anisotropic layer (L_{A1}) and the material constants of the anisotropic layer (ε_A,δ_A).

Fig. 5 shows the sequence of convergence of the dispersion relation for a degenerate band edge point for optimization using one variable L_V to recover the known solution, confirming the robustness of the method and the computed solution.

In Table 2, we display other solutions found by using different parameters for the optimizations. We observe that the thickness of the vacuum layer remains approximately the same for all sets, while the thickness of anisotropic layer varies. The first derivative and the second derivative of all sets are less than 1.0e-10, which is sufficiently small to make the phenomena distinctive in the time domain.

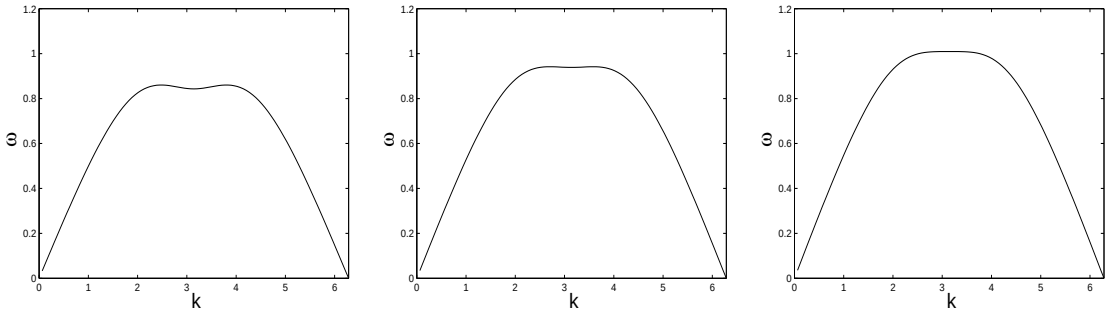

Figure 5: Snapshots from the optimization of a degenerate bandgap crystal with one variable L_V. L_V=0.3029 (left), 0.3994 (center), 0.4589 (right) after 6 iterations, $\frac{d\omega}{dx}$= 2.6258e-015, $\frac{d^2\omega}{dx^2}$= 1.3466e-013 with $\lambda = 100$.

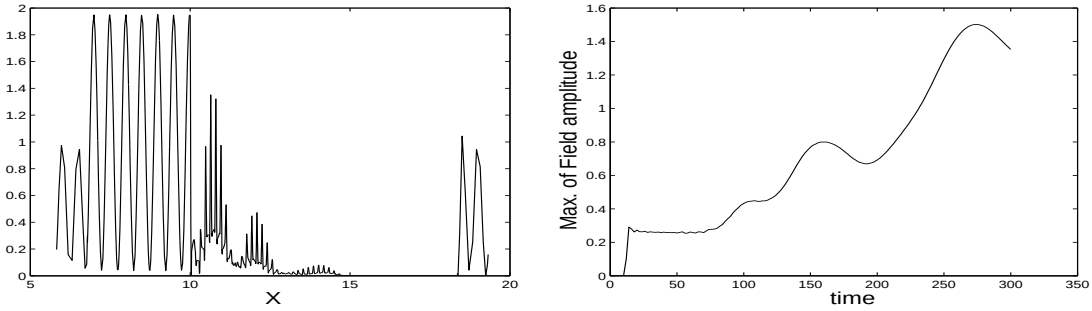

Figure 6: Field amplitude (left) and maximum of field amplitude (right) of degenerate band edge with parameter set 1 of Table 2. The number of unit cells is 32.

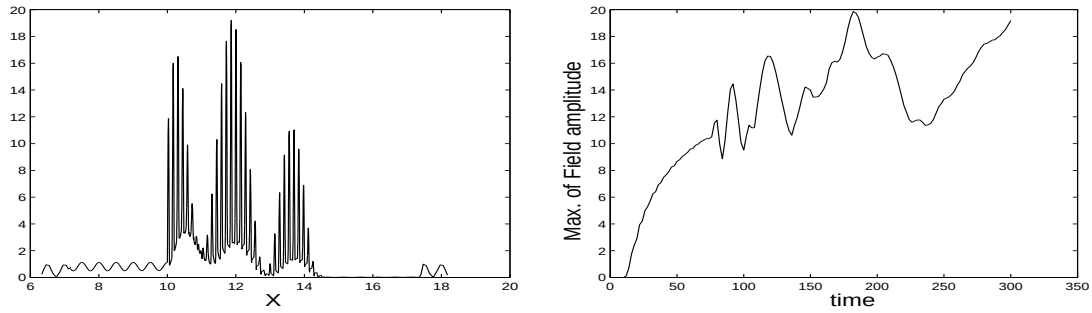

Figure 7: Field amplitude (left) and maximum of field amplitude (right) of degenerate band edge with parameter set 4 of Table 2. The number of unit cells is 32.

However, one significant difference is that the transmittance of set 4 is significantly larger than for the other sets. This is in some contrast to the commonly held belief that high reflectance is inevitable for a degenerate band edge crystal.

Figs. 6 and 7 show the field amplitude at $T = 300.0$ and the increase of the maximum field amplitude with parameter Set 1 and Set 4 from Table 2. These figures clearly display the significance of large transmittance at the degenerate band edge, highlighting the potential benefits of a fully automatic design approach.

Table 2: Optimized solutions with different number of parameters or different initial values for the degenerate band edge. Other parameters are the same as those in Table 1.

		Set 1	Set 2	Set 3	Set 4
Input	n	1	2	2	4
	variables	$L_V(L_{A1}=L_{A2})$	L_V,L_{A1}	L_V,L_{A1}	L_V,L_{A1},ε_A, δ_A
	ϕ_2	$\pi/4$	$\pi/4$	$\pi/3$	$\pi/4$
Solution	L_V	0.45890	0.46000	0.45005	0.45005
	L_{A1}	0.27055	0.29190	0.43633	0.45050
	ε_A	5.1	5.1	5.1	7.0
	δ_A	1.1	1.1	1.1	3.92
	ω_0	1.00940	1.01331	1.11726	0.88645
	k_0	π	π	π	π
	$\frac{d\omega}{dk}\|_{\omega=\omega_0}$	2.9175e-16	2.9063e-16	0*	4.3189e-15
	$\frac{d^2\omega}{dk^2}\|_{\omega=\omega_0}$	6.0364e-14	1.3414e-13	1.5102e-013	3.8326e-10
	TR	0.0064	0.0070	0.0440	0.3474

5 Optimization and design of oblique frozen mode crystals

As proposed by Figotin and Vitebsky [5, 6], stationary inflection points can be also generated without magnetic layers and with structures even simpler as the degenerate band gap structures. To achieve this goal, one needs to break the symmetry and consider incident waves at oblique angles. When an oblique incident waves propagates into a periodic layer consisting of one anisotropic layer with $\varepsilon_{xz} \neq 0$ ($\varepsilon_{xz} = xz$-component of permittivity tensor $\hat{\varepsilon}$) and vacuum, one can observe a similar but weaker frozen mode inside the layer as compared to the gyrotropic crystal.

However, the crystal parameters in [5, 6] were computed by a one dimensional transfer matrix method based on a tangential consistency assumption of the wave to eliminate the derivatives in the (x, y)-plane, i.e.,

$$\frac{d\hat{E}}{dx} = ik_{x,y}\hat{E} = \left(\frac{k_{x,y}}{\omega}\right) i\omega\hat{E} = \left(\frac{k_{x,y}}{\omega}\right)\left(-\frac{d\hat{E}}{dt}\right),$$

where $k_{x,y}$ is the component of the wave vector $\vec{k}$ in the (x, y)-plane and ω is the frequency of the incident plane wave. The frozen mode was studied in [1], after enforcing the above consistency in Maxwell's equations. However, the existence of the oblique frozen mode in real three dimension remains open since the consistency assumption is artificial. To model this general case, the transfer matrix method is not applicable and we must solve the full Maxwell eigenvalue problems for the dispersion relation.

The solution of this more complicated problem can be computed with a general frequency domain solver [14]. In addition to choosing a wave vector $\vec{k}_0$ for the stationary inflection point ω_0, we need to choose a band containing ω_0. For example, ω_0 exists on the second band and the first band for the magnetic frozen mode and degenerate band

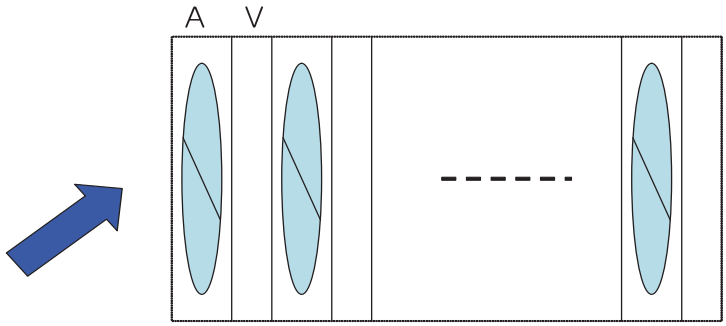

Figure 8: Array of crystals displaying the oblique frozen mode. The periodic structure consists of one anisotropic layer (A) with $\varepsilon_{xz}\neq 0$ and vacuum (V) between them. The incident wave needs to propagate into the layer at an oblique angle.

edge respectively, but for the oblique frozen mode, no such information is known in advance. To identify the band where ω_0 exist, we search whole bands for a wave vector $\vec{k}_0$ such as

$$\min_j \left| \sum_{j=-2}^{2} \frac{d\omega}{dk}(\vec{k}_j) \right| < \delta, \quad \delta = \text{small number}.$$

To increase the speed of the search process, we preselect several bands in advance which appear to have $\vec{k}_0$ satisfying the above condition. As for parameters for the optimization, we use the oblique angle of incident wave ($k_x = k_y$), the thickness of the vacuum layer (L_V) and the material constants of the anisotropic layer (ε_{11},ε_{33}) with the material constants given as

$$\hat{\varepsilon}_A = \begin{bmatrix} \varepsilon_{11}\cos\theta^2 + \varepsilon_{33}\sin\theta^2 & 0 & (\varepsilon_{11}-\varepsilon_{33})\cos\theta\sin\theta \\ 0 & \varepsilon_{22} & 0 \\ (\varepsilon_{11}-\varepsilon_{33})\cos\theta\sin\theta & 0 & \varepsilon_{33}\cos\theta^2 + \varepsilon_{11}\sin\theta^2 \end{bmatrix}.$$

Among several stationary inflection points found by optimization, one of them with the lowest frequency ω_0 is given as follows (also see Fig. 9):

$$\begin{aligned} &\theta = \pi/4, \quad \varepsilon_{11} = \varepsilon_{22} = 4.66812966, \quad \varepsilon_{33} = 3.9656, \quad L_V = 0.5711535, \\ &\vec{k} = (-0.4800309, -0.4800309, -0.008982), \quad \omega_0 = 1.295439(c/L), \\ &\left.\frac{d\omega}{dk}\right|_{\omega=\omega_0} = 0.00048279, \quad \left.\frac{d^2\omega}{dk^2}\right|_{\omega=\omega_0} = 0.004393. \end{aligned}$$

The dispersion relation resulting from the new parameters clearly show the correct properties for the three-dimensional crystal.

5.1 Time-domain modeling of the 3D crystal

To observe the frozen mode phenomenon in three dimension, the new set of optimized parameters is solved in a time-domain wave propagation model with periodic boundary

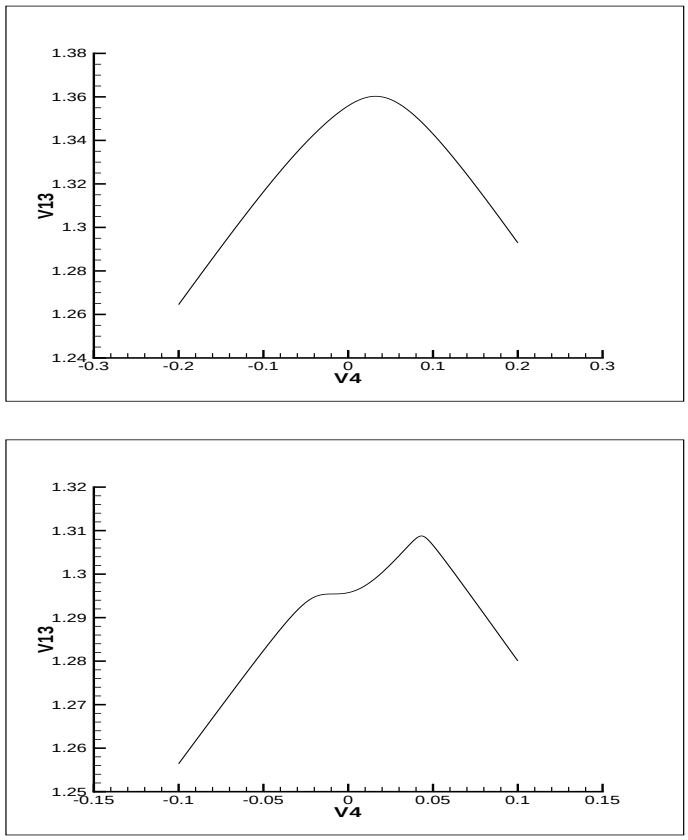

Figure 9: Dispersion relation for the three-dimensional Maxwell eigenvalue problem with material parameters from paper [6] (top), and with the optimized solution for the 8th band (bottom). A stationary inflection point ω_0 is observed in the dispersion relation only with the optimized solution.

condition in the (x, y)-plane and absorbing boundary condition (ABC) used along the z-direction to avoid reflection of the outgoing waves. The general setup is illustrated in Fig. 10.

We assume that ε_{xz} is the only non-zero off-diagonal element for permittivity tensor $\hat{\varepsilon}$, resulting in Maxwell's equations taking the form

$$\begin{bmatrix} \frac{\partial \tilde{E}_z}{\partial y} - \frac{\partial \tilde{E}_y}{\partial z} \\ \frac{\partial \tilde{E}_x}{\partial z} - \frac{\partial \tilde{E}_z}{\partial x} \\ \frac{\partial \tilde{E}_y}{\partial x} - \frac{\partial \tilde{E}_x}{\partial y} \end{bmatrix} = -\frac{\partial}{\partial t} \begin{bmatrix} \tilde{H}_x \\ \tilde{H}_y \\ \tilde{H}_z \end{bmatrix},$$

$$\begin{bmatrix} \frac{\partial \tilde{H}_z}{\partial y} - \frac{\partial \tilde{H}_y}{\partial z} \\ \frac{\partial \tilde{H}_x}{\partial z} - \frac{\partial \tilde{H}_z}{\partial x} \\ \frac{\partial \tilde{H}_y}{\partial x} - \frac{\partial \tilde{H}_x}{\partial y} \end{bmatrix} = \begin{bmatrix} \varepsilon_{xx} & 0 & \varepsilon_{xz} \\ 0 & \varepsilon_{yy} & 0 \\ \varepsilon_{xz} & 0 & \varepsilon_{zz} \end{bmatrix} \frac{\partial}{\partial t} \begin{bmatrix} \tilde{E}_x \\ \tilde{E}_y \\ \tilde{E}_z \end{bmatrix}.$$

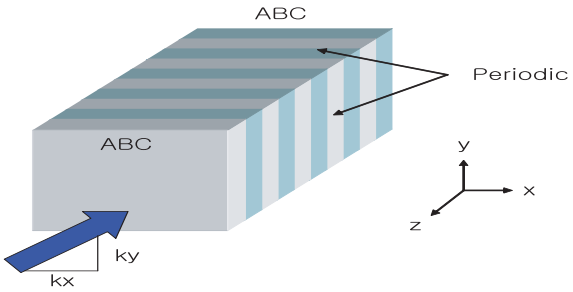

Figure 10: Wave propagation problem with periodic boundary condition along x and y direction with ABC at the end of z direction. The incident wave propagates into the layer at an oblique angle.

Assuming (x,y)-periodicity we express $\tilde{E}$ and $\tilde{H}$ as two dimensional Fourier series

$$\tilde{E}(x,y,z,t) = \sum_{m_y=-N_y/2}^{N_y/2} \sum_{m_x=-N_x/2}^{N_x/2} E(m_x,m_y,z,t) e^{im_x \frac{2\pi}{L_x} x} e^{im_y \frac{2\pi}{L_y} y},$$
$$\tilde{H}(x,y,z,t) = \sum_{m_y=-N_y/2}^{N_y/2} \sum_{m_x=-N_x/2}^{N_x/2} H(m_x,m_y,z,t) e^{im_x \frac{2\pi}{L_x} x} e^{im_y \frac{2\pi}{L_y} y}.$$

Here N_x, N_y are number of points along the x and y direction, and L_x and L_y are lengths of the domain along the x and y direction, respectively. Note that L_x and L_y depend on the angle of incidence of plane wave. By substituting these expansions into the above Maxwell's equations, including also the absorbing boundary conditions in the z-direction, we have

$$\begin{bmatrix} (im_y)E_z - \frac{\partial E_y}{\partial z} \\ \frac{\partial E_x}{\partial z} - (im_x)E_z \\ (im_x)E_y - (im_y)E_x \end{bmatrix} = i\omega \begin{bmatrix} s_z & 0 & 0 \\ 0 & s_z & 0 \\ 0 & 0 & 1/s_z \end{bmatrix} \begin{bmatrix} H_x \\ H_y \\ H_z \end{bmatrix},$$
$$\begin{bmatrix} (im_y)H_z - \frac{\partial H_y}{\partial z} \\ \frac{\partial H_x}{\partial z} - (im_x)H_z \\ (im_x)H_y - (im_y)H_x \end{bmatrix} = -i\omega \begin{bmatrix} \varepsilon_{xx} & 0 & \varepsilon_{xz} \\ 0 & \varepsilon_{yy} & 0 \\ \varepsilon_{xz} & 0 & \varepsilon_{zz} \end{bmatrix} \begin{bmatrix} s_z & 0 & 0 \\ 0 & s_z & 0 \\ 0 & 0 & 1/s_z \end{bmatrix} \begin{bmatrix} E_x \\ E_y \\ E_z \end{bmatrix},$$

where ω is the frequency of the incident plane wave and the PML parameter, s_z, is defined as $s_z = 1+\sigma_z/(i\omega)$ with σ_z being a parabolic absorption profile [18]. This yields the time-domain Maxwell's equations

$$\frac{\partial H_x}{\partial t} = \frac{\partial E_y}{\partial z} - (im_y)E_z - \sigma_z H_x, \quad \frac{\partial H_y}{\partial t} = -\frac{\partial E_x}{\partial z} + (im_x)E_z - \sigma_z H_y,$$
$$\frac{\partial B_z}{\partial t} = -(im_x)E_y + (im_y)E_x, \quad \frac{\partial H_z}{\partial t} = \frac{\partial B_z}{\partial t} + \sigma_z B_z,$$

$$
\begin{aligned}
D_\varepsilon \frac{\partial E_x}{\partial t} &= -\varepsilon_{zz}\{\frac{\partial H_y}{\partial z} - (im_y)H_z\} + \varepsilon_{xz}\{(im_y)H_x - (im_x)H_y\} - \sigma_z E_x, \\
\varepsilon_{yy}\frac{\partial E_y}{\partial t} &= \frac{\partial H_x}{\partial z} - (im_x)H_z - \sigma_z E_y, \\
D_\varepsilon \frac{\partial D_z}{\partial t} &= \varepsilon_{xz}\{\frac{\partial H_y}{\partial z} - (im_y)H_z\} - \varepsilon_{xx}\{(im_y)H_x - (im_x)H_y\}, \\
\frac{\partial E_z}{\partial t} &= \frac{\partial D_z}{dt} + \sigma_z D_z,
\end{aligned}
$$

which must be solved for all combinations of the Fourier modes, i.e., $m_x \leq |N_x/2|$, $m_y \leq |N_y/2|$. We have also for simplicity defined the determinant

$$D_\varepsilon = \varepsilon_{xx}\varepsilon_{zz} - \varepsilon_{xz}^2.$$

To discretize along the z-direction, we use a discontinuous Galerkin method, similar to what is discussed in detail in [1,2]. For the time marching, we implement an implicit scheme for the linear derivatives along z direction and explicit scheme for the remainder [15,16]. To validate the code, the transmittance and refraction angle are computed for a plane incident wave propagating from vacuum to a dielectric material at various oblique angles. As shown in Fig. 11, the scheme reproduces the expected behavior with high accuracy.

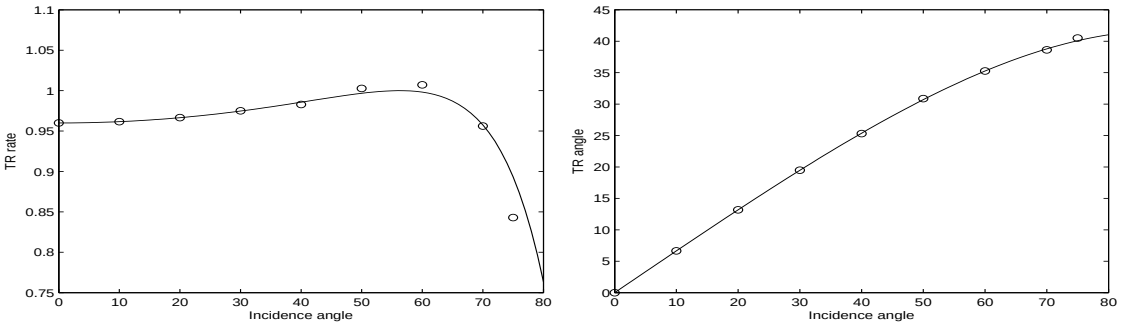

Figure 11: Results for 3D time domain modeling test. Transmittance vs. incidence angle (left), transmittance angle vs. incidence angle (right). The solid line indicates the exact value and the circles indicate computed values.

In Fig. 12, we show the energy density flux ($\frac{1}{\mu_0}(\mathbf{E}\times\mathbf{B})$) and the field amplitude ($|\mathbf{E}|^2 + |\mathbf{H}|^2$) with the optimized parameter values and observe several features of the frozen mode. We define the energy density flux difference (EDFD) [1]

$$\text{EDFD} = \int_S \mathbf{e}_f \cdot n ds = \int_V \nabla \mathbf{e}_f dV, \quad \mathbf{e}_f = \text{energy density flux.}$$

This indicates the amount of energy density inside the layer per unit time. In Fig. 13 we observe a significant value of the EDFD along the z direction between the first cell

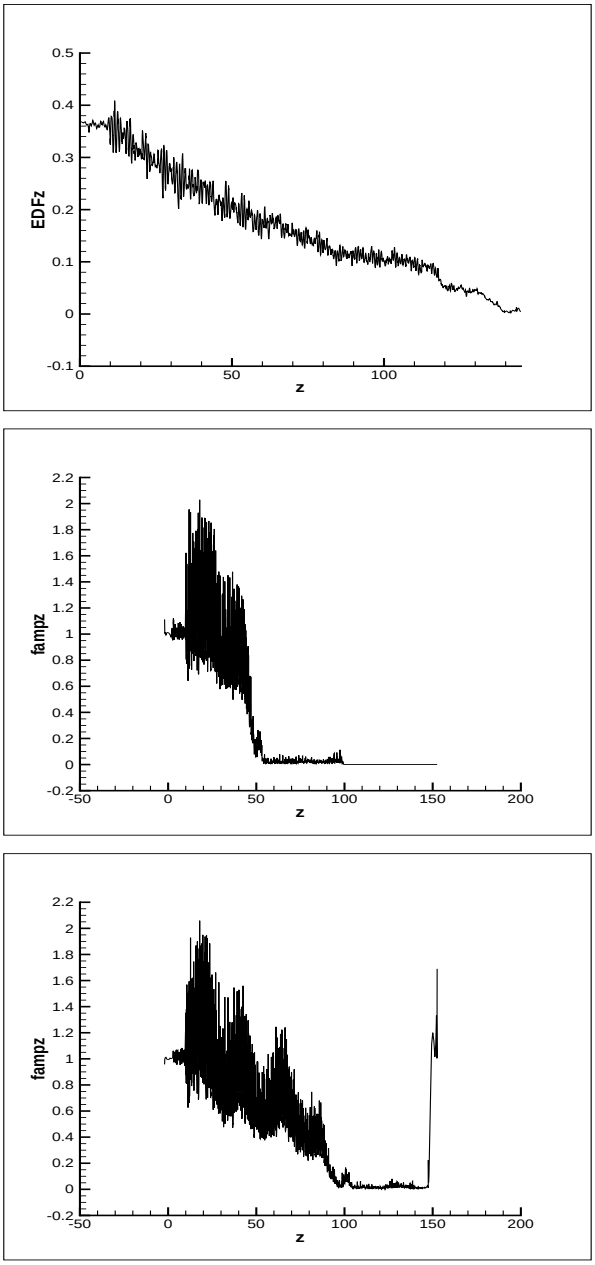

Figure 12: Energy density flux (top) and the field amplitude with optimized parameters at T=100 (middle) and at T=200 (bottom), $N_x = N_y = 6$, $N_z = 12$, (N_x, N_y, N_z)=number of grid points along (x, y, z). Number of unit cells is 100.

and the last cell (the right part of Fig. 13). This reflects an increased field amplitude, compressed energy density and the slow-down of the wave. However, each of these phenomena are weaker than that of the magnetic frozen mode as also observed in [1].

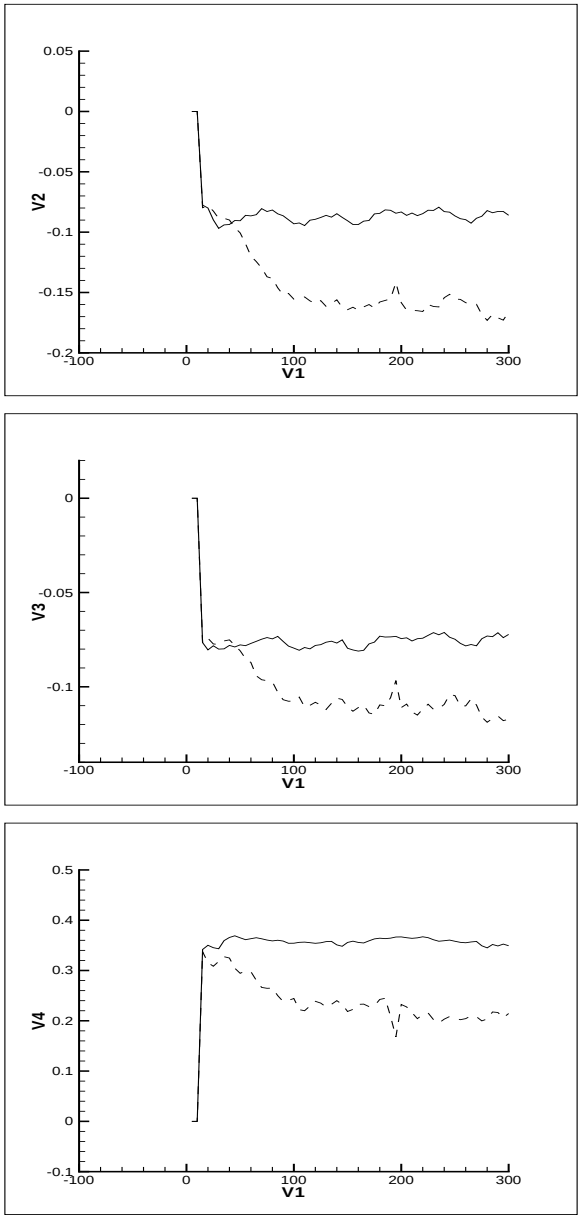

Figure 13: Energy Flux Density Difference (EDFD) between the first cell and the last cell along x (top), y (middle), z (bottom) direction. Solid line is with optimized parameters, dashed line is with original values. $N_x = N_y = 6$, $N_z = 12$, Number of unit cell=64.

Fig. 13 also compares the EDFD for all directions for the crystals based on the original values and the optimized parameter values. With the optimized values, we observe that the EDFD in the (x,y)-plane is close to zero, indicating very limited energy flux in that plane while the EDFD along the z direction remains high even after a long time. With

original values, the EDFD in the (x,y)-plane remains nontrivial, which may serve as an explanation for the lack of a frozen mode the original configuration due to significant leakage of energy in the (x,y)-plane.

6 Conclusion

We have explored the use of PDE constrained optimization for the design and optimization of photonic crystals exhibiting a frozen mode behavior. This phenomenon is related to the existence of Van Hove singularities in the dispersion relation. We have demonstrated the ability to recover known solutions and computed several new sets of parameters by optimizing the geometry and/or the materials of the crystals. For both of the magnetic frozen mode and degenerate band edge, each sets of parameters obtained by optimization with different number of variables show the generally similar phenomena, but some features are different. Above all, the transmittance, which is a crucial element for the energy density and field amplitude inside the crystal, varies significantly. In particular one set for the degenerate band edge displays a transmittance of 1/3, which is more than 50 times larger than previous realizations.

For the case with the frozen mode requiring an oblique illumination, we succeed in finding a stationary inflection point in three dimensions with parameters' sets derived by nonlinear optimization. The existence of the frozen mode in three dimension is shown, but the phenomena themselves are not as distinctive as in the previous two instances. One possible reason can be the intrinsic property of the oblique array which makes the wave vector k_0 close to zero.

The current computational design tool allows one to specify materials and/or geometries, and seek to design crystals with the sought-after properties, if they exist. The computations shown here illustrate that the Van Hove singularities are found broadly in the dispersion relations, indicating that many configurations often exist. Future works may include finding stationary inflection points or degenerate band edge points showing strong frozen mode in 2 or 3 dimensional structures or in crystal configurations consisting of more types of materials. One natural goal is to seek configurations with improved broad band behavior.

Acknowledgments

This work was supported by the U.S. Air Force Office of Scientific Research under the grant FA9550-04-1-0359.

References

[1] S. Chun and J. S. Hesthaven, Modeling of the frozen mode phenomenon and its Sensitivity using Discontinuous Galerkin methods, Commun. Comput. Phys., 2 (2007), 611-639.

[2] J. S. Hesthaven and T. Warburton, Nodal high-order methods on unstructured grids, J. Comput. Phys., 182 (2002), 186-221.
[3] A. Figotin and I. Vitebsky, Nonreciprocal magnetic photonic crystals, Phys. Rev. E, 63 (2001), 0666609.
[4] A. Figotin and I. Vitebsky, Electromanetic unidirectionality in magnetic photonic crystals, Phys. Rev. B, 67 (2003), 165210.
[5] A. Figotin and I. Vitebsky, Oblique frozen modes in periodic layered media, Phys. Rev. E, 68 (2003), 036609.
[6] J. Ballato, A. Ballato, A. Figotin and I. Vitebsky, Frozen light in periodic stacks of anisotropic layers, Phys. Rev. E, 71 (2005), 1.
[7] L. Van Hove, Van Hove singularities, Phys. Rev., 89 (1953), 1189.
[8] M. Ibanescu, S. G. Johnson, D. Roundy, C. Luo, Y. Fink and J. D. Joannopoulos, Anomalous disperion relations by symmetry breaking in axially uniform waveguides, Phys. Rev. Lett., 92 (2004), 6.
[9] K. Svanberg, The method of moving asymptotes: A new method for structural optimization, Int. J. Numer. Meth. Engrg., 24 (1987), 359-373.
[10] C. Zillober, A globally convergent version of the method of moving asymptotes, Struct. Optimiz., 6 (1993), 166-174.
[11] W. H. Zhang, C. Fleury, P. Duysinx, V. H. Nguyen and I. Laschet, A generalized method of moving asymptotes (GMMA) including equality constraints, Struct. Optimiz., 12 (1996), 143-146.
[12] K. Svandberg, A new globally convergent version of MMA, Technical Report TRITA-MAT-1999-OS2, Dept. of Mathematics, KTH, Stockholm, 1999.
[13] K. Svanberg, Two primal-dual interior-point methods for the MMA subproblems, Technical Report TRITA-MAT-1998-OS12, Dept. of Mathematics, KTH, Stockholm, 1998.
[14] S. G. Johnson and J. D. Joannopoulos, Block-iterative frequency-domain methods for Maxwell's equations in a planewave basis, Opt. Express, 8 (2001), 173-190.
[15] U. M. Ascher, S. J. Ruuth and R. J. Spiteri, Implicit-explicit Runge-Kutta methods for time-dependent partial differential equations, Appl. Numer. Math., 25 (1997), 151-167.
[16] C. A. Kennedy and M. H. Carpenter, Additive Runge-Kutta schemes for convection-diffusion-reaction equations, Appl. Numer. Math., 44 (2003), 139-181.
[17] A. Figotin and I. Vitebskiy, Gigantic transmission and band-edge resonance in periodic stacks of anisotropic layers, Phys. Rev. E, 72 (2005), 036619.
[18] A. Taflove and S. C. Hagness, Computational Electrodynamics, the Finite-Difference Time-Domain Method, 3rd Ed., Artech House, Boston, 2005.